Received April 14, 2022, accepted May 15, 2022, date of publication May 18, 2022, date of current version May 26, 2022.

Digital Object Identifier 10.1109/ACCESS.2022.3176320

A Novel Channel Model and Optimal Power Control Schemes for Mobile mmWave Two-Tier Networks

JOYDEV GHOSH[1], HUSEYIN HACI[2], NEERAJ KUMAR[3,4,5,6], (Senior Member, IEEE), KHALED A. AL-UTAIBI[7], (Member, IEEE), SADIQ M. SAIT[8], (Senior Member, IEEE), AND CHAKCHAI SO-IN[9], (Senior Member, IEEE)

[1]School of Computer Science and Robotics, Tomsk Polytechnic University, 634050 Tomsk, Russia
[2]Department of Electrical and Electronics Engineering, Near East University, 1403 Nicosia, Turkey
[3]Department of Computer Science and Engineering, Thapar Institute of Engineering & Technology, Patiala 147004, India
[4]Department of Computer Science and Information Engineering, Asia University, Taichung City 413, Taiwan
[5]School of Computer Science, University of Petroleum and Energy Studies, Dehradun, Uttarakhand 248007, India
[6]Department of Computer Science and Information Systems, King Abdulaziz University, Jeddah 22254, Saudi Arabia
[7]Computer Science and Software Engineering Department, University of Ha'il, Ha'il 53962, Saudi Arabia
[8]Department of Computer Engineering, King Fahd University of Petroleum & Minerals, Dhahran 31261, Saudi Arabia
[9]Department of Computer Science, College of Computing, Khon Kaen University, Khon Kaen 40002, Thailand

Corresponding authors: Joydev Ghosh (joydev.ghosh.ece@gmail.com) and Chakchai So-In (chakso@kku.ac.th)

This work was supported in part by Khon Kaen University.

ABSTRACT We present a unified system model and framework for the analytical performance study of two heterogeneous and physically-distinct, but coexisting, networks that work harmoniously at the same time, space, and frequency domains. The two-tier network model considered in this paper is an overlaying of femtocells on a macrocell. Overlaying femtocells improves the performance by offloading traffic from macrocells and providing spatial diversity. The mmWave channel model employed considers the number of clusters and rays within each cluster to vary due to the end-user mobility. This is a new and different model compared to the widely used channel models for mmWave two-tier networks. Optimal power control is formulated as a sum-rate maximization problem for downlink and uplink transmissions at two-tier networks and a power allocation scheme is proposed by following Shannon-Hartley theorem. A comprehensive and interesting performance investigation is provided, where it is shown that the upper bound on the number of admitted secondary users has a linear relationship with the outage probability threshold, logarithmic relationship with SINR and exponential relationship with channel gain factors. Simulation results show that the proposed scheme with sub-channel iterative Lagrange multipliers search algorithm is very effective at managing the cross-tier interference and can outperform a competitive scheme from literature that is based on cognitive radio technology. The computational complexity analysis of proposed algorithms are also given, since the complexity of second algorithm can be a performance-complexity trade-off issue for systems with limited computation power and time requirements.

INDEX TERMS Mobile mmwave channel model, optimal power control, optimal spectrum sensing, mmwave two-tier networks.

I. INTRODUCTION

The fifth-generation (5G) networks and the internet of things (IoT) promise to transform our lives. They will connect billions of devices and enable everything from driver-less cars to smart-homes, offices, cities, and the world. In order to enable these applications, much faster and more reliable communications are needed compared to the current fourth generation (4G) networks. It is envisioned that a 100x increase in area capacity compared to long-term evolution (LTE) networks will be required in 5G [1]. Multi-tier networks that overlay each other with heterogeneous radio technologies and physical properties are a promising technology that can minimize coverage gaps, provide spatial diversity gain and support the ultra-high data traffic demand of hot-spots in future mmWave Systems [2]. A popular

The associate editor coordinating the review of this manuscript and approving it for publication was Tiago Cruz.

example of multi-tier networks is the two-tier Macro-Femtocell networks [3]–[5].

It is shown that while designing such a multi-tier network, the co-channel operation of macrocells and femtocells can result in inter-tier interference that may worsen the performance if appropriate interference cancellation techniques are not employed [6], [7]. One of the basic solutions to mitigate interference in a two-tier network is by defining one tier to consist of macro users (MUs), also called as primary users (PUs), and the other to consist femto users (FUs), also called as secondary users (SUs), who have cognitive potential to detect unoccupied channels [8], [9]. In [10], a spectrum split up method is utilized to reduce the cross-tier interference between macrocell and femtocell networks, named as fractional frequency reuse (FFR) method. FFR can be achieved by dividing up the entire available spectrum into multiple sub-bands and putting a constraint on access over the femtocell networks to achieve interference coordination [11]–[14].

A popular technique to provide better network coverage and data transmission reliability is to employ large-scale antenna arrays (LSAA) to achieve strong directional beamforming gain that can avoid interference signals between geographically distributed users in mobile mmWave massive MIMO [15]. Although prior channel state information (CSI) at the transmitter is an important factor in the implementation, the increased dimensionality of channel matrices due to LSAA at the transmitter causes unacceptably large beam training overhead, serious pilot contamination in massive MIMO and higher computational complexity [16]. The authors in [17]–[22] presented the path-loss model and MIMO channel model for line-of-sight (LoS) and non-LoS (NLoS) case studies, and characterized angular-spread models for intracluster (multipath component distribution) and intercluster (cluster distribution) evolving across a LSAA with the Laplacian and Gaussian distributions at millimetre-length electromagnetic waves.

In [23], a full-duplexing (FD) based interference alignment (IA) algorithm for small cell network operation has been proposed that can significantly improve the spectral efficiency (SE). Minimize spectrum consumption clustering (MSCC) and minimize interference leakage clustering (MILC) schemes are employed for IA to mitigate inter- and intra-cluster interferences. A Zadoff-Chu (ZC) sequence based scheme that is feasible even for ultra-dense networks (UDN) and massive MIMO settings was presented in [24] for signal spreading in conjunction with the proposed $\alpha - \eta - k - \mu$ fading model.

In [24], [25] interference mitigation scenarios to deal with various challenges such as doppler shift, blockage effect, power of the scattered waves and non-linearity of the space are studied. Doppler shifts in terms of angle of arrivals (AoAs) and angle of departures (AoDs) of the signal were compensated under beamforming network to develop a quasi time-invariant mmWave MIMO channel similar to [28]–[35]. Besides interference mitigation, radio resource management plays a crucial role in achieving high performance in next generation networks [36]. [37]–[41] considered Lagrangian dual decomposition technique in orthogonal frequency division multiple access (OFDMA)-based femtocell heterogeneous networks (HetNets) to design various optimization problems on power allocation, subchannel assignment, user association, load balancing and spectrum sharing subject to delay-sensitive (DS) and delay-tolerant (DT) constraints.

The work in [42] utilized mmWave FBSs to optimize the network throughput and microwave MBSs to improve energy efficiency (EE). Compared to the presented data-aided (DA) estimator for multicell decoupled two-tier femtocell networks in [43], [44] studied downlink (DL) and uplink (UL) decoupling (DUDe) in HetNets and presented significantly better performance. For the data-driven decision making in two-tier self-organizing networks (SONs), machine learning is considered in [45], where Distributed Cooperative Q-Learning (DCQL) scheme is used for power allocation in densely deployed femtocells and demonstrated much improved EE.

Further [46] proposed a deep reinforcement learning (RL) based scheme to manage the DL interference and significantly improved the system capacity. In [47], authors investigated coverage probability over Rician fading channels by considering Marcum Q-function for unmanned aerial vehicles (UAVs) assisted femtocell networks and validated its energy-efficient solution. Licensed assisted access (LAA) based small cell networks have been proposed in [48] to maximize the network throughput while FBSs share licensed and unlicensed channels with MBSs and Wi-Fi, respectively, where closed form expressions are established with the exchange of Lagrangian parameters through joint power and channel allocations. Other interesting research work on dragonfly, ant lion, modified firefly and ABC optimization algorithms are provided by [49]–[51].

Despite these interesting researches, the channel model considered in the aforementioned studies assumes the number of clusters and rays within each cluster to be fixed [54], [55]. However, in mobile mmWave massive MIMO based communications, the number of clusters and rays within each cluster varies due to user mobility [52]. In case the mmWave channel is not accurately modeled and appropriate signal processing is performed at the receiver, the received signal's quality may be significantly degraded, resulting in unreliable and slow communications. To address these open issues, in this paper we consider a novel channel model that has not been studied for mmWave two-tier networks before and propose optimal power control schemes for mobile mmWave massive MIMO based two-tier networks. The contributions of this paper are listed as follows:

- A closed-form mathematical expression for a novel channel model at mmWave two-tier networks is formulized, where the variable number of clusters and rays within each cluster is modeled by well-known probability distributions.
- An optimal power control scheme that employs a multi-channel iterative lower-bound coefficients search

algorithm is proposed to jointly maximize the sum-rate of DL and UL transmissions at mobile mmWave two-tier networks. Two lemmas are given and proved to obtain the optimal power allocation solution. Lemma 1 is used to transform the non-convex power allocation problem into its convex approximation and lemma 2 is given to prove that the transformed problem is strictly convex over given channel pairs.

The rest of the paper is organized as follows. In Section II, we present a system model considering co-existence scenario with FBSs deployment at MBS cell edge area in order to improve the network's quality of service (QoS) and formulate an optimization problem by following Shannon–Hartley theorem to maximize capacity for both UL and DL subject to the power constraints. To solve the issue of power regulation for the dense deployment of femtocells, new analytical derivations are provided along with a few properties in the form of lemmas in Section III. Then, two computationally tractable algorithms focusing on a large number of sub-channels and the iterative water-filling method are applied along with comparative complexity analysis. Simulation results are presented in Section IV. The paper is concluded with some remarks in Section V.

TABLE 1. The notations of main network parameters.

Symbol	Description
N_{MU}	Number of macro users
N_{FU}	Number of femto users
N_M	Number of macro base stations (MBSs)
N_F	Number of femto base stations (FBSs)
ϱ_m, ϱ_f and ϱ_e	Deployment intensity of MBSs, FBSs and at cell edges respectively
α	Path-loss exponent
ξ	Path-loss gain
x	The network entity that facilitates the communication service to a given user
$d_{n,i,k}$	3D distance between k^{th} BS and i^{th} UE on n^{th} sub-band at t time instant
ς	Bernoulli random variable
Z	Clusters associated with each transmission link regardless of MBS or FBS scattering paths
Y	Rays between transmitter and receiver for the number of clusters $z < Z$
h^x_{zy}	Multi-path channel fading of Rician type
K	Rician shape parameter
T_s	Sampling period
M	Number of symbols in a single data frame
$\hat{f}_d$	An expected value of Doppler frequency shift due to velocity
f_c	Carrier frequency
N_{sc}	Number of sub-channels in each sub-band
μ	Channel estimation error

II. SYSTEM MODEL

We assume a cellular network comprising super high frequency (SHF) macro base station (MBS) and mmWave femto base stations (FBSs). The UL and DL characteristics of a two-tier HetNet have been investigated. The MBS operates on the sub-6 GHz frequency band and the FBSs are deployed along the cell edge area, see Figure 1. FBS assists in improving the system capacity and also provides secondary network coverage service, i.e., as a backup coverage to MBSs, by jointly sharing sub-6GHz and mmWave bands. Femtocells underlaid macrocell network with joint operation at sub-6GHz and mm-wave bands play a key role to avoid outage and open up new opportunities to enable beyond fifth-generation (B5G) networks for the industrial internet of things (IIoT). At the same time, this type of operation may cause severe co- and cross-tier interferences, hence, there is a need for well interference management [24].

MBSs are deployed as a homogeneous poisson point process (HPPP) with intensity $\varrho_m \in \mathbb{R}^2$. The cell edges are modeled as a PPP with intensity $\varrho_e \in [0, 2\pi] \times \mathbb{R}^+$. The deployment of FBSs along the cell edge side is assumed to be a PPP with intensity $\varrho_f \in \mathbb{R}^+$. If the distance between a user and an accessible nearby LOS MBS is denoted by d_{ml}, then this notation changes to d_{mn} for the NLOS MBS located at the closed proximity. Likewise, d_{fl} and d_{fn} are the notations used to denote the distance from a user to a LOS FBS or a NLOS FBS, respectively, located at the closed proximity. Therefore, the distributions of d_{ml}, d_{mn}, d_{fl} and d_{fn} for y as the location of the user at the associated BS can be expressed by [53]

$$f_{d_{ml}}(y) = 2\pi\varrho_m y e^{-\pi\varrho_m y^2}, \quad y < r_m, \tag{1}$$

$$f_{d_{mn}}(y) = 2\pi\varrho_m y e^{-\pi\varrho_m (y^2 - r_m^2)}, \quad y > r_m, \tag{2}$$

$$f_{d_{fl}}(y) = 2\varrho_f e^{-2\varrho_f y}, \tag{3}$$

$$f_{d_{fn}}(y) = 2\pi\varrho_e F_{d_{fn}}(y) \left[2\varrho_f y \int_0^y \frac{e^{-2\varrho_f \sqrt{y^2 - r_f^2}}}{\sqrt{y^2 - r_f^2}} dr_f \right], \tag{4}$$

where r_m denotes macrocell LOS radius; and r_f denotes femtocell LOS radius; $F_{d_{fn}}(y)$ denotes cumulative distribution function (CDF) and can be expressed by

$$F_{d_{fn}}(y) = e^{2\pi\varrho_e \left(y - \int_0^y e^{-2\varrho_f \sqrt{y^2 - r_f^2}} dr_f \right)}. \tag{5}$$

Let symbol x to indicate the network entity that facilitates the communication service to a given user, where $x = f$ if the user is connected to a FBS and $x = m$ if the user is connected to a MBS. Then, path-loss between k^{th} BS and i^{th} UE on n^{th} sub-band can be expressed as below,

$$\Xi^x_{n,i,k} = \xi d^{\alpha}_{n,i,k}, \tag{6}$$

where ξ indicates path-loss gain at a reference distance $a_{n,i,k,t} = 1$; $d_{n,i,k} = \sqrt{a^2_{n,i,k,t} + b^2_{n,i,k,t}}$ denotes the three dimensional (3D) distance between k^{th} BS and i^{th} UE on n^{th} sub-band at t time instant; $a_{n,i,k,t}$ denotes the distance between k^{th} BS and i^{th} UE on n^{th} sub-band at t time instant; $b_{n,i,k,t}$ is used to denote absolute antenna height difference between k^{th} BS and i^{th} UE on n^{th} sub-band at t time instant; α is assumed for path-loss exponent which characterizes the LOS and NLOS path-loss exponents and can be expressed as follows: $\alpha \triangleq \varsigma d_{n,i,k}\breve{\alpha} + [1 - \varsigma d_{n,i,k}]\hat{\alpha}$ where $\varsigma \in \{1, 0\}$ is

a Bernoulli random variable and it is becoming 1 if there is non-existence of NLOS components else 0; $\breve{\alpha}$ and $\hat{\alpha}$ are representing LOS and NLOS path-loss exponents, respectively, of a BS.

In this system model, suppose each transmission link consists of Z clusters regardless of MBS or FBS scattering paths. We also assume that there is Y rays between transmitter and receiver for the number of clusters $z \leq Z$ [52]. Therefore, the channel matrix belongs to each link can be expressed as,

$$H^x_{n,i,k} = \sum_{z=1}^{Z(t)} \sum_{y=1}^{Y_{Z(t)}} h^x_{zy} F^x_{R_x}(\theta^x_{R_x,zy}) v^x_{R_x}(\theta^x_{R_x,zy}) F^x_{T_x}(\theta^x_{T_x,zy}) \times v^{x^\star}_{T_x}(\theta^x_{T_x,zy}), \quad (7)$$

where $Z(t) \sim \max\{Poisson(\zeta), 1\}$, [52, refer to (6)] and $Y_{Z(t)} \sim \mathbb{D}(1, Z)$ [52, refer to (11)] such properties of the mmWave channel are discussed in [54] and [55] and studied in [52]; $v^x_{R_x}$ and $v^x_{T_x}$ are used to denote 3D spatial response vector for the equipped antennas at the transmitter and receiver; $v^{x^\star}_{T_x}$ represents complex conjugate of spatial response vector $v^x_{T_x}$; $F^x_{R_x}$ and $F^x_{T_x}$ denote field factors that cause antenna gain in the channel computation; $\theta^x_{R_x,zy}$ and $\theta^x_{T_x,zy}$ represent horizontal AoA and horizontal AoD related to each ray that associated to each of Z clusters; h^x_{zy} denotes multi-path channel fading of Rician type and can be expressed by

$$h^x_{zy} = \sqrt{\frac{m_{zy}K}{K+1}}[h^x_{zy}]_d + \sqrt{\frac{m_{zy}}{K+1}}[h^x_{zy}]_s, \quad (8)$$

where m_{zy} denotes the average channel gain at n^{th} sub-band for the channel fading function related to baseband signal and $m_{zy} = \mathbb{E}\{|h^x_{zy}(n)|^2\}$; K indicates Rician shape parameter; $[h^x_{zy}]_d$ and $[h^x_{zy}]_s$ are considered for direct- and scattered-paths of the desired transmission link and they can be expressed as follows:

$$[h^x_{zy}]_d = \exp(-j\eth^x_{n,i,k}) \quad (9)$$

$$[h^x_{zy}]_s = \frac{1}{A_{T_x}} \sum_{l=1}^{A_{T_x}} \exp(2\pi \hat{f}_d m T_s - j\zeta), \; m = \{1, 2, \cdots, M\}, \quad (10)$$

where $\eth^x_{n,i,k}$ is an arbitrary numerical value during the computation and it is dependent only on the distance between i^{th} UE and k^{th} BS; A_{T_x} denotes number of equipped transmit antennas at the transmitter and the baseband signal is supposed to be modulated with the sampling period T_s keeping M symbols in a single data frame; ζ is an arbitrary phase shift that uniformly distributed over $[0, 2\pi]$, $\hat{f}_d = \mathbb{E}\{f_d\}$ be the expected value of Doppler frequency shift due to velocity v in which $E\{.\}$ is the statistical expectation operator and $f_d = \frac{f_c v}{c}\cos\phi$ where ϕ is uniformly distributed over $[-\frac{\omega}{2}, \frac{\omega}{2}]$; f_c denotes carrier frequency; c stand for velocity of light.

The contribution of beamforming gain in the received signal strength (RSS) from a BS to a UE can be estimated by

$$[G^x_{n,i,k}]_d = |B^x_{T_x} H^x_{n,i,k} (B^x_{R_x})^T|^2, \quad (11)$$

where $B^x_{T_x}$ and $(B^x_{R_x})^T$ denote beamforming vector at the T_x and transpose of beamforming vector at the R_x.

[56] presents a heterogeneous network with a MBS positioned at the centre and and 4 FBSs positioned under the network coverage of MBS at the cell edge area, particularly located at $(2, 2), (-2, 2), (-2, -2), (2, -2)$. The total number of MUs denoted by N_{MU} is randomly positioned under the network coverage area of MBS. A co-existence scenario where a large number of femtocells implanted at cell edge area of macrocell network but this consideration is not much useful to achieve the objective due to involving of interference effect. Figure 1 deals with a network where FBSs are deployed under the network coverage of MBS and use the same band of frequency with macrocell. This work exclusively focus on the analysis of UL/DL transmissions alongside a bit discussion of UL/DL transmissions.

Here, the two-tier network based on OFDMA technique incorporates N_M number of MBSs and N_F number of FBSs in a cell. The assigned BW at edge area of the network coverage of MBS is divided up into three sub-bands by employing the FFR method [57,58]. One sub-band can incorporate a number of sub-channels denoted by N_{SC} and they are accessible to facilitate the users positioned at the area near to the cell-centre and the area belong to the cell edge by means of network service.

Thus, SINR,[1] denoted by $\gamma^x_{n,i,k}$, of a typical user positioned at the middle taking the network service from the MBSs or FBSs can be written as:

$$\gamma^x_{n,i,k} = \frac{\Xi^x_{n,i,k}[G^x_{n,i,k}]_d}{I^x_{n,i,k} + I^{x'}_{n,i,k} + \sigma^2_{n,i,k}}, \quad (12)$$

where

$$I^f_{n,i,l} = \sum\nolimits_{l=1,l\neq k}^{N_M} \Xi^m_{n,i,l}[G^m_{n,i,l}]_I, \quad \forall l \in \{1, 2, \ldots, N_M\};$$

$$I^{f'}_{n,i,j} = \sum\nolimits_{j=1}^{N_M \times N_F} \varkappa^n_j \Xi^f_{n,i,j}[G^f_{n,i,j}]_I, \quad \forall j \in \{1, 2, \ldots, N_F\};$$

$$I^m_{n,i,l} = \sum\nolimits_{l=1}^{N_M} \Xi^m_{n,i,l}[G^m_{n,i,l}]_I, \quad \forall l \in \{1, 2, \ldots, N_M\};$$

$$I^{m'}_{n,i,j} = \sum\nolimits_{j=1,j\neq k}^{N_M \times N_F} \varkappa^n_j \Xi^f_{n,i,j}[G^f_{n,i,j}]_I, \quad \forall j \in \{1, 2, \ldots, N_F\};$$

$I^x_{n,i,k}$ and $I^{x'}_{n,i,k}$ are denoted as co-tier and cross-tier interferences respectively, where $\Xi^x_{n,i,l}$ and $[G^x_{n,i,k}]_d$, used to define transmit power and beamforming gain of the desired signal respectively. $\varkappa^n_j \in \{1, 0\}$ assumes to be 1 if n^{th} sub-channel is allocated to FBS j, else 0. The co-tier interference takes place among the network elements of the same types (e.g., between adjacent femtocells) and the cross-tier interference occurs among network elements that belong to different

[1]The probability density function (PDF) of SINR can be expressed as below,

$$f_{PDF} = \frac{1}{2\sqrt{\mu}\bar{\gamma}^x_{n,i,k}}\left(\exp\left(-\frac{y}{(1+\sqrt{\mu})\bar{\gamma}^x_{n,i,k})}\right) - \exp\left(-\frac{y}{(1-\sqrt{\mu})\bar{\gamma}^x_{n,i,k})}\right)\right), \; y \geq 0;$$

where μ denotes channel estimation error and $\bar{\gamma}^x_{n,i,k}$ denotes average SINR.

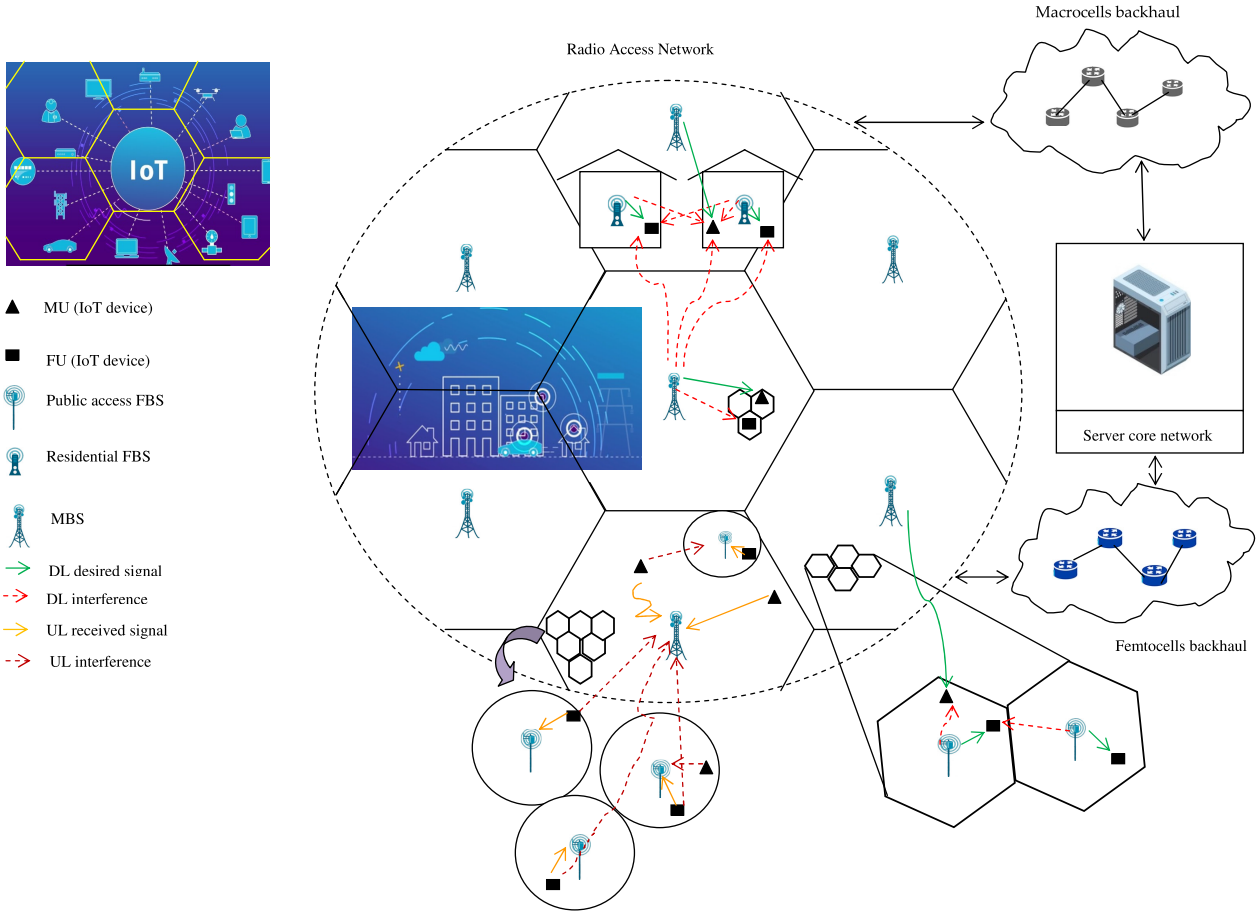

FIGURE 1. **A millimeter-wave mobile broadband (MMB) network, where MBS acts as MMB base station and FBSs co-exist within the hexagon network coverage with densely deployed IoT devices.**

tiers (e.g., between a macrocell and a femtocell). They can be used interchangeably based on whether $x = f$ or $x = m$. Additive White Gaussian noise (AWGN) is denoted for noise power by $\sigma^2_{n,i,k}$.

Problem Formulation:

Case I (For $x = m$): The case where a user is connected to a MBS. By following (12), the SINR of i^{th} MU located at k^{th} MBS on n^{th} sub-channel can be expressed as,

$$\gamma^{m(DL)}_{n,i} = \frac{p_{n,k} G_{n,i,k}}{I^{m(DL)}_{n,i,k} + I^{m(DL)\star}_{n,i,k} + \sigma^2_{n,i,k}}. \tag{13}$$

Likewise, the SINR at k^{th} MBS for i^{th} MUs on n^{th} sub-channel can be expressed as,

$$\gamma^{m(UL)}_{n,k} = \frac{p_{n,i} G_{n,i,k}}{I^{m(UL)}_{n,i,k} + I^{m(UL)\star}_{n,i,k} + \sigma^2_{n,i,k}}. \tag{14}$$

Based on Shannon Hartley capacity formula [59], the DL and UL capacity for $x = m$ can be written as,

$$C^{DL}_{MU} = \sum_{i=1}^{N_M} \sum_{n=1}^{N_{sc}} \Psi_{n,i} B \log_2(1 + \gamma^{m(DL)}_{n,i}). \tag{15}$$

Let each MBS consists, $b = \frac{N_{MU}}{N_M}$

$$C^{UL}_{MBS} = \sum_{k=1}^{N_{MU}} \sum_{n=1}^{N_{sc}} \Psi_{n,k} B \log_2(1 + \gamma^{m(UL)}_{n,k}). \tag{16}$$

Case II (For $x = f$): The case where a user is connected to a FBS. By following (12), the SINR of j^{th} FU located at l^{th} FBS on n^{th} sub-channel can be expressed as,

$$\gamma^{f(DL)}_{n,j} = \frac{p_{n,l} G_{n,j,l}}{I^{f(DL)}_{n,j,l} + I^{f(DL)\star}_{n,j,l} + \sigma^2_{n,j,l}}. \tag{17}$$

Likewise, the SINR at l^{th} FBS for the FUs on n^{th} sub-channel can be expressed as,

$$\gamma^{f(UL)}_{n,l} = \frac{p_{n,j} G_{n,j,l}}{I^{f(UL)}_{n,j,l} + I^{f(UL)\star}_{n,j,l} + \sigma^2_{n,j,l}}. \tag{18}$$

Based on Shannon Hartley capacity formula, the DL and UL capacity for $x = f$ can be written as,

$$C^{DL}_{FU} = \sum_{j=1}^{N_F} \sum_{n=1}^{N_{sc}} \Phi_{n,j} B \log_2(1 + \gamma^{f(DL)}_{n,j}). \tag{19}$$

Let each FBS consists, $d = \frac{N_{FU}}{N_F}$

$$C_{MBS}^{UL} = \sum_{l=1}^{N_{FU}} \sum_{n=1}^{N_{sc}} \Phi_{n,l} B \log_2(1 + \gamma_{n,l}^{f(UL)}). \tag{20}$$

Now, we formulate the capacity maximization problem for the macro-femto heterogeneous networks as follows:

$$\underset{\{\Psi_{n,i},\Psi_{n,k},\Phi_{n,j},\Phi_{n,l},p_k,p_i,p_l,p_j\}}{\arg\min} \{C_{MU}^{DL} + C_{MBS}^{UL} + C_{FU}^{DL} + C_{FBS}^{UL}\}, \tag{21}$$

Subject to:

$$\gamma_{n,i}^{m(DL)} \geq \gamma_{th1}, \gamma_{n,k}^{m(UL)} \geq \gamma_{th1}, \quad \forall n \in N_{sc}, \; i \in N_M, k \in N_{MU}, \tag{21.a}$$

$$\gamma_{n,j}^{f(DL)} \geq \gamma_{th2}, \gamma_{n,l}^{f(UL)} \geq \gamma_{th2}, \quad \forall n \in N_{sc}, \; j \in N_F, l \in N_{FU}, \tag{21.b}$$

$$\Psi_{n,a} + \Psi_{n,a+1} \geq 1, \quad \forall n \in N_{sc}, a \in N_M, \tag{21.c}$$

$$\Psi_{n,a} + \Psi_{n,a-1} \geq 1, \quad \forall n \in N_{sc}, a \in N_M, \tag{21.d}$$

$$\Psi_{n,b} + \Psi_{n,b+1} \leq 1, \quad \forall n \in N_{sc}, b \in \frac{N_{MU}}{N_M}, \tag{21.e}$$

$$\Psi_{n,b} + \Psi_{n,b-1} \leq 1, \quad \forall n \in N_{sc}, b \in \frac{N_{MU}}{N_M}, \tag{21.f}$$

$$\Phi_{n,c} + \Phi_{n,c+1} \geq 1, \quad \forall n \in N_{sc}, c \in N_F, \tag{21.g}$$

$$\Phi_{n,c} + \Phi_{n,c-1} \geq 1, \quad \forall n \in N_{sc}, c \in N_F, \tag{21.h}$$

$$\Phi_{n,d} + \Phi_{n,d+1} \leq 1, \quad \forall n \in N_{sc}, d \in \frac{N_{FU}}{N_F}, \tag{21.i}$$

$$\Phi_{n,d} + \Phi_{n,d-1} \leq 1, \quad \forall n \in N_{sc}, d \in \frac{N_{FU}}{N_F}, \tag{21.j}$$

$$\sum_{n=1}^{N_{sc}} p_{n,a} \leq p_{max1}, \quad \forall n \in N_{sc}, a \in N_M, \tag{21.k}$$

$$\sum_{n=1}^{N_{sc}} p_{n,b} \leq p_{max2}, \quad \forall n \in N_{sc}, b \in \frac{N_{MU}}{N_M}, \tag{21.l}$$

$$\sum_{n=1}^{N_{sc}} p_{n,c} \leq p_{max3}, \quad \forall n \in N_{sc}, c \in N_F, \tag{21.m}$$

$$\sum_{n=1}^{N_{sc}} p_{n,d} \leq p_{max4}, \quad \forall n \in N_{sc}, d \in \frac{N_{FU}}{N_F}, \tag{21.n}$$

where p_{max1}, p_{max2}, p_{max3} and p_{max4} are maximal powers of an MBS, an MU, an FBS and an FU, respectively.

Given the capacity optimization problem, next section provides the analytical derivations for power control and two search algorithms for the optimal solution, along with their complexity analysis.

III. POWER REGULATION ON CHANNEL PAIRS

While femtocells are operated in close proximity for high-density deployment scenarios, co-tier interference becomes the main concern for the network performance although the ideal channel allocation technique can ensure controlled interference irrespective of co-tier or cross-tier to satisfy the QoS requirements.

Suppose that $\mho_{n_1}$ and $\mho_{n_2}$ be the set of links between the FBS and the FU can perform the operation of communication on the channel pair n_1 and n_2. Similarly, φ_{n_1} and φ_{n_2} assume to be the set of links between MBS and MU on the same channel pair. Now, achievable sum-rate on the given channel pair can be expressed as follows,

$$\begin{aligned} R(p_{n,k}, p_{n,i}, p_{n,l}, p_{n,j}) &= \sum_{i=1}^{N_M} \sum_{j=1}^{N_F} \sum_{n=1}^{N_{sc}} \log_2(1 + \gamma_{n,i}^{m(DL)}) \\ &+ \log_2(1 + \gamma_{n,k}^{m(UL)}) + \log_2(1 + \gamma_{n,j}^{f(DL)}) \\ &+ \log_2(1 + \gamma_{n,l}^{f(UL)}). \end{aligned} \tag{22}$$

As sum-rate maximization maximizes the capacity in the cognitive femtocell networks, hence, sum-rate maximization problem employing power control can be expressed as follows:

$$P1: \underset{\{p_{n,k},p_{n,i},p_{n,l},p_{n,j}\}}{\arg\min} \{\mathbb{E}[R(p_{n,k}, p_{n,i}, p_{n,l}, p_{n,j})]\}, \tag{23}$$

Subject to: $n \in \{n_1, n_2\}$, $\{i, k, j, l\} \in \{\mho_{n_1} \cup \mho_{n_2} \cup \varphi_{n_1} \cup \varphi_{n_2}\}$ and power constraints (21k)-(21n); where $\mathbb{E}[]$ indicates the expectation over the channel pair. $\gamma_{n,i}^{m(DL)}$, $\gamma_{n,k}^{m(UL)}$, $\gamma_{n,j}^{f(DL)}$ and $\gamma_{n,l}^{f(UL)}$ are provided by (13), (14), (17) and (18), respectively. The sets $\mho_{n_1}, \mho_{n_2}, \varphi_{n_1}$ and φ_{n_2} are decided by $\Psi_{n,i}, \Psi_{n,k}, \Phi_{n,j}, \Phi_{n,l}$, respectively. Only the power constraints (21k)-(21n) parts are taken into account by assuming the fulfilment of QoS needs with proper channel allocation.

The problem of selecting a set of cochannel users and allocating power among them to maximize the weighted system sum rate subject to a given power constraint is shown to be a non-convex combinatorial problem [60-62]. Such problems can be transformed into a convex problem by deriving the tightest lower-bound of the logarithmic function of weighted system sum rate [60-62]. Thus, the problem $P1$ given in (23) is not a strictly convex problem due to the fact that (22) is a non-concave function. Therefore, in order to achieve universal optimum of $P1$, it is the necessary condition that $P1$ should be a convex optimization problem.

In the following sections, we propose flexible power control scheme to obtain the solution over the channel pair.

A. FLEXIBLE POWER CONTROL SCHEME

For the proposed flexible power control scheme, we derive and employ the concave property, i.e., tightest lower-bound of $\log_2(1 + u)$ for $u \geq 0$, to get the optimal solution of non-convex problem $P1$. In this context, the below lemma [60] is a useful lower-bound solution to transform the $P1$ problem into a convex approximation.

Lemma 1: A lower bound inequality of the logarithmic function is written by,

$$\log_2(1 + u) \geq \psi \log_2 u + \phi, \text{ for } u \geq 0;$$

where ψ and ϕ denote lower bound co-efficients and are given by,

$$\psi = \frac{u_0}{1+u_0},$$
$$\phi = \log_2(1+u_0) - \frac{u_0}{1+u_0}\log_2 u_0, \text{ for } u_0 \geq 0.$$

However, $\psi \log_2 u + \phi$ is very close to $\log_2(1+u)$ and the lower bound is tight and equal to $\log_2(1+u)$ at $u = u_0$. ■

By Lemma 1, $P1$ can be extended to a new problem as given below:

$$P2: \underset{\{p_{n,k},p_{n,i},p_{n,l},p_{n,j}\}}{\arg\min} \{\mathbb{E}[R_1(p_{n,k},p_{n,i},p_{n,l},p_{n,j})]\},$$
$$\text{Subject to: } n \in \{n_1,n_2\},\ \{i,k,j,l\} \in \{\mathfrak{V}_{n_1} \cup \mathfrak{V}_{n_2} \cup \varphi_{n_1} \cup \varphi_{n_2}\},$$
$$\text{Power constraints } (21k)\text{-}(21n), \quad (24)$$

where $R_1(p_k,p_i,p_l,p_j)$ is given by (25), as shown at the bottom of the page, in which $\psi_{n,i}^{[t]}$, $\psi_{n,k}^{[t]}$, $\psi_{n,j}^{[t]}$, $\psi_{n,l}^{[t]}$, $\phi_{n,i}^{[t]}$, $\phi_{n,k}^{[t]}$, $\phi_{n,j}^{[t]}$, $\phi_{n,l}^{[t]}$, $\gamma_{n,i}^{m(DL)[t]}$, $\gamma_{n,k}^{m(UL)[t]}$, $\gamma_{n,j}^{f(DL)[t]}$ and $\gamma_{n,l}^{f(UL)[t]}$ represent lower bound co-efficients and DL/UL SINR corresponding to n^{th} sub-channel at t^{th} iteration.

With the assumption of $\bar{p}_{n,k} = \log_2(p_{n,k})$, $\bar{p}_{n,i} = \log_2(p_{n,i})$, $\bar{p}_{n,l} = \log_2(p_{n,l})$ and $\bar{p}_{n,j} = \log_2(p_{n,j})$, $R_1(p_{n,k}, p_{n,i}, p_{n,l}, p_{n,j})$ is re-expressed as a concave function in (26), as shown at the bottom of the page. Then, we transform P_2 into a new problem P_3 as follows:

$$P3: \underset{\{p_{n,k},p_{n,i},p_{n,l},p_{n,j}\}}{\arg\min} \{\mathbb{E}[R_2(\bar{p}_{n,k},\bar{p}_{n,i},\bar{p}_{n,l},\bar{p}_{n,j})]\}, \quad (27)$$
$$\text{Subject to:}$$
$$\sum_{n=1}^{N_{sc}} p_{n,k} \leq p_{max1}, \quad \forall n \in N_{sc}, k \in N_M, \quad (27.a)$$
$$\sum_{n=1}^{N_sc} p_{n,i} \leq p_{max2}, \quad \forall n \in N_{sc}, i \in \frac{N_{MU}}{N_M}, \quad (27.b)$$
$$\sum_{n=1}^{N_{sc}} p_{n,l} \leq p_{max3}, \quad \forall n \in N_{sc}, l \in N_F, \quad (27.c)$$
$$\sum_{n=1}^{N_{sc}} p_{n,j} \leq p_{max4}, \quad \forall n \in N_{sc}, j \in \frac{N_{FU}}{N_F}, \quad (27.d)$$

Lemma 2: The problem P3 is a strictly convex over given channel pair.

Proof: In order to describe the local curvature of a function of multiple variables with the help of Hessian matrix, we consider $s(x_1,x_2) = s(\bar{p}_{n,k},\bar{p}_{n,i}) = \log_2(I_{n,i,k}^{m(DL)} + I_{n,i,k}^{m(DL)\star} + \sigma_{n,i,k}^2) + \log_2(I_{n,i,k}^{m(UL)} + I_{n,i,k}^{m(UL)\star} + \sigma_{n,i,k}^2)$. If all second partial derivatives of s exist and are continuous over the domain of the function, then the Hessian matrix H_s of s is a square 2×2 matrix and can be defined and arranged as follows:

$$H_s = \begin{bmatrix} \frac{\partial^2 s}{\partial x_1^2} & \frac{\partial^2 s}{\partial x_1 x_2} \\ \frac{\partial^2 s}{\partial x_2 x_1} & \frac{\partial^2 s}{\partial x_2^2} \end{bmatrix} = \begin{bmatrix} s_{11} & s_{12} \\ s_{21} & s_{22} \end{bmatrix}.$$

By applying the Sylvesters criterion [63], the strict concavity of $s(x_1,x_2)$ can achieve on the space spanned by (x_1,x_2) for $s_{11} > 0$ and $s_{11}s_{22} - s_{12}s_{21} > 0$. Likewise, $\log_2(I_{n,j,l}^{f(DL)} + I_{n,j,l}^{f(DL)\star} + \sigma_{n,j,l}^2) + \log_2(I_{n,j,l}^{f(DL)} + I_{n,j,l}^{f(DL)\star} + \sigma_{n,j,l}^2)$ is also a strictly concave function. Hence, (26) can be said to be a strictly concave/convex by obeying the law given in [64] which is any non-negatively weighted sum of concave functions remains concave. Therefore, Lemma 2 follows. ■

An optimization problem $P3$ with constraints given in (27) that describe the boundary of the region can solve by applying the method of Lagrange multipliers and the Lagrangian is given by

$$L(\tilde{p}, \lambda_n^{1[t]}, \lambda_n^{2[t]}, \lambda_n^{3[t]}, \lambda_n^{[4[t]})$$
$$= \mathbb{E}[R_2(\bar{p}_{n,k},\bar{p}_{n,i},\bar{p}_{n,l},\bar{p}_{n,j})]$$
$$\pm \sum_{n=1}^{N_{sc}} \lambda_n^{1[t]}(p_{n,k} - p_{max1}) \pm \sum_{n=1}^{N_{sc}} \lambda_n^{2[t]}(p_{n,i} - p_{max2})$$

$$R_1(p_{n,k},p_{n,i},p_{n,l},p_{n,j}) \triangleq \sum_{i=1}^{N_M}\sum_{j=1}^{N_F}\sum_{n=1}^{N_{sc}}\Big\{\psi_{n,i}^{[t]}\log_2(\gamma_{n,i}^{m(DL)[t]}) + \phi_{n,i}^{[t]} + \psi_{n,k}^{[t]}\log_2(\gamma_{n,k}^{m(UL)[t]}) + \phi_{n,k}^{[t]} + \psi_{n,j}^{[t]}\log_2(\gamma_{n,j}^{f(DL)[t]}) + \phi_{n,j}^{[t]} + \psi_{n,l}^{[t]}\log_2(\gamma_{n,l}^{f(UL)[t]}) + \phi_{n,l}^{[t]}\Big\}. \quad (25)$$

$$\begin{aligned} R_2(\bar{p}_{n,k},\bar{p}_{n,i},\bar{p}_{n,l},\bar{p}_{n,j}) = \sum_{i=1}^{N_M}\sum_{j=1}^{N_F}\sum_{n=1}^{N_{sc}}\Big\{ & \phi_{n,i}^{[t]} + \psi_{n,i}^{[t]}[\bar{p}_{n,k} + \log_2(G_{n,i,k}^{[t]}) - \log_2(I_{n,i,k}^{m(DL)[t]} + I_{n,i,k}^{m(DL)\star[t]} + \sigma_{n,i,k}^{2[t]})] \\ & + \phi_{n,k}^{[t]} + \psi_{n,k}^{[t]}[\bar{p}_{n,i} + \log_2(G_{n,i,k}^{[t]}) - \log_2(I_{n,i,k}^{m(UL)[t]} + I_{n,i,k}^{m(UL)\star[t]} + \sigma_{n,i,k}^{2[t]})] \\ & + \phi_{n,j}^{[t]} + \psi_{n,j}^{[t]}[\bar{p}_{n,l} + \log_2(G_{n,j,l}^{[t]}) - \log_2(I_{n,j,l}^{f(DL)[t]} + I_{n,j,l}^{f(DL)\star[t]} + \sigma_{n,j,l}^{2[t]})] \\ & + \phi_{n,l}^{[t]} + \psi_{n,l}^{[t]}[\bar{p}_{n,j} + \log_2(G_{n,j,l}^{[t]}) - \log_2(I_{n,j,l}^{f(UL)[t]} + I_{n,j,l}^{f(UL)\star[t]} + \sigma_{n,j,l}^{2[t]})]\Big\} \end{aligned} \quad (26)$$

$$\pm \sum_{n=1}^{N_{sc}} \lambda_n^{3[t]}(p_{n,l} - p_{max3}) \pm \sum_{n=1}^{N_{sc}} \lambda_n^{4[t]}(p_{n,j} - p_{max4}), \quad (28)$$

where $\tilde{p} = [\bar{p}_{n,k}, \bar{p}_{n,i}, \bar{p}_{n,l}, \bar{p}_{n,j}]$ denotes approximation vector; $\lambda_n^{1[t]}$, $\lambda_n^{2[t]}$, $\lambda_n^{3[t]}$, and $\lambda_n^{4[t]}$ are Lagrange multipliers.[2]

The Lagrange function is

$$g(\lambda_n^{1[t]}, \lambda_n^{2[t]}, \lambda_n^{3[t]}, \lambda_n^{4[t]}) = \underset{\{\bar{p}_{n,k}, \bar{p}_{n,i}, \bar{p}_{n,l}, \bar{p}_{n,j}\}}{\arg\max} L(\tilde{p}, \lambda_n^{1[t]}, \lambda_n^{2[t]}, \lambda_n^{3[t]}, \lambda_n^{4[t]}), \quad (29)$$

and the Lagrange problem with fixed $\psi^{[t]}$ and $\phi^{[t]}$ is

$$P5: \underset{\{\lambda_n^{1[t]}, \lambda_n^{2[t]}, \lambda_n^{3[t]}, \lambda_n^{4[t]}\}}{\arg\max} g(\lambda_n^{1[t]}, \lambda_n^{2[t]}, \lambda_n^{3[t]}, \lambda_n^{4[t]}), \quad (30)$$

Subject to: $\lambda_n^{1[t]} \geq 0$,[3] $\lambda_n^{2[t]} \geq 0$, $\lambda_n^{3[t]} \geq 0$, $\lambda_n^{4[t]} \geq 0$, where $\psi^{[t]} = [\psi_{n,i}^{[t]}, \psi_{n,k}^{[t]}, \psi_{n,j}^{[t]}, \psi_{n,l}^{[t]}]$ and $\phi^{[t]} = [\phi_{n,i}^{[t]}, \phi_{n,k}^{[t]}, \phi_{n,j}^{[t]}, \phi_{n,l}^{[t]}]$ denotes approximation vectors.

By following the 1^{st}-order necessary conditions of equality and inequality constrained problem, we derive the near optimal stationary power points of (28) with respect to $\bar{p}_{n,k}$ keeping $\lambda_n^{1[t]}$ fixed,

$$\frac{\partial L}{\partial \bar{p}_{n,k}} = 0 \overset{(a)}{=} \psi_{n,i}^{[t]} \pm \lambda_n^{1[t]} p_{n,k} \log_e 2, \quad (31)$$

where (a) follows the property given in (32).

$$\frac{\partial}{\partial \bar{p}_{n,k}} \left(2^{\bar{p}_{n,k}}\right) = 2^{\bar{p}_{n,k}} \log_e 2 = p_{n,k} \log_e 2, \quad (32)$$

where, $\bar{p}_{n,k} = \log_2(p_{n,k})$.

[2]The Lagrange multiplier is a real number, so it doesn't matter if we use $\pm\lambda$ for exact equality constraints but '+' is the preferred sign for an inequality constraint, $r(p_1, p_2) \leq 0$.

[3]**Lower bound property:** If $\lambda_n^{1[t]} \geq 0$, then $g(\lambda_n^{1[t]}, \lambda_n^{2[t]}, \lambda_n^{3[t]}, \lambda_n^{4[t]}) \leq \tilde{p}^{\star}$

Proof: If $\tilde{p}$ is feasible and $\lambda_n^{1[t]} \geq 0$, then

$\mathbb{E}[R_2(\tilde{p})] \geq L(\tilde{p}, \lambda_n^{1[t]}, \lambda_n^{2[t]}, \lambda_n^{3[t]}, \lambda_n^{4[t]}) \geq \arg\max_{\{\tilde{p}\}} L(\tilde{p}, \lambda_n^{1[t]}, \lambda_n^{2[t]}, \lambda_n^{3[t]}, \lambda_n^{4[t]})$.

Hence, maximizing over all feasible $\tilde{p}$ implies $g(\lambda_n^{1[t]}, \lambda_n^{2[t]}, \lambda_n^{3[t]}, \lambda_n^{4[t]}) \leq \tilde{p}^{\star}$. ■

Based on the expressions in (31), the following equations of the near optimal stationary power points at iteration $(t+1)$ hold,

$$\begin{cases} p_{n,k}^{[t+1]} = \dfrac{\psi_{n,i}^{[t]}}{\lambda_n^{1[t]} \log_e 2}, \\ p_{n,i}^{[t+1]} = \dfrac{\psi_{n,k}^{[t]}}{\lambda_n^{2[t]} \log_e 2}, \\ p_{n,l}^{[t+1]} = \dfrac{\psi_{n,j}^{[t]}}{\lambda_n^{3[t]} \log_e 2}, \\ p_{n,j}^{[t+1]} = \dfrac{\psi_{n,l}^{[t]}}{\lambda_n^{4[t]} \log_e 2}. \end{cases} \quad (33)$$

We propose multi-channel iterative lower-bound coefficients search (MC-ILBCS) algorithm in order to determine the optimum lower-bound coefficients with the initialization $\psi^{[1]} = 1$ and $\phi^{[1]} = 0$ to perform in high-SINR approximation, where $\psi^{[t]}$ and $\phi^{[t]}$ denote the t^{th} estimation for ψ and ϕ, respectively.

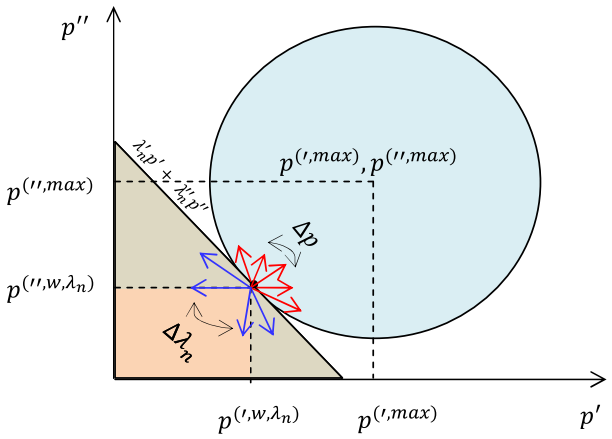

FIGURE 2. The power plane illustration for two-users.

For a pair of users, (26) can be reformulated as in (34), as shown at the bottom of the page, where $\tilde{p}' = [\bar{p}'_{n,k}, \bar{p}'_{n,i}, \bar{p}'_{n,l}, \bar{p}'_{n,j}]$ and $\tilde{p}'' = [\bar{p}''_{n,k}, \bar{p}''_{n,i}, \bar{p}''_{n,l}, \bar{p}''_{n,j}]$ denote approximation vectors; $w = \{w', w''\}$ indicates set of weights for data rates of the users; $\lambda_n^{'[t]} = \{\lambda_n^{1'[t]}, \lambda_n^{2'[t]}, \lambda_n^{3'[t]}, \lambda_n^{4'[t]}\}$ and $\lambda_n^{''[t]} = \{\lambda_n^{1''[t]}, \lambda_n^{2''[t]}, \lambda_n^{3''[t]}, \lambda_n^{4''[t]}\}$ represent set of assigned Lagrange multipliers in the context of user-pair.

$$\begin{aligned} \underset{\{\tilde{p}', \tilde{p}''\}}{\arg\max} \Bigg[& \mathbb{E}[w' R_2'(\tilde{p}')] + \mathbb{E}[w'' R_2''(\tilde{p}'')] + \sum_{n=1}^{N_{sc}} \lambda_n^{1'[t]}(p'_{n,k} - p^{(',max1)}) + \sum_{n=1}^{N_{sc}} \lambda_n^{2'[t]}(p'_{n,i} - p^{(',max2)}) \\ & + \sum_{n=1}^{N_{sc}} \lambda_n^{3'[t]}(p'_{n,l} - p^{(',max3)}) + \sum_{n=1}^{N_{sc}} \lambda_n^{4'[t]}(p'_{n,j} - p^{(',max4)}) + \sum_{n=1}^{N_{sc}} \lambda_n^{1''[t]}(p''_{n,k} - p^{('',max1)}) + \sum_{n=1}^{N_{sc}} \lambda_n^{2''[t]}(p''_{n,i} - p^{('',max2)}) \\ & + \sum_{n=1}^{N_{sc}} \lambda_n^{3''[t]}(p''_{n,l} - p^{('',max3)}) + \sum_{n=1}^{N_{sc}} \lambda_n^{4''[t]}(p''_{n,j} - p^{('',max4)}) \Bigg], \end{aligned} \quad (34)$$

Algorithm 1 Multi-Channel Iterative Lower-Bound Coefficients Search

1. Initialize $t = 1$, $\psi^{[1]} = 1$ and $\phi^{[1]} = 0$
2. Compute $\tilde{p}$ as the solution to the concave problem (28)
3. Update $p_{n,k}^{[t+1]}$, $p_{n,i}^{[t+1]}$, $p_{n,l}^{[t+1]}$ and $p_{n,j}^{[t+1]}$ according to (33)
4. Compute $\gamma^{[t]}$ according to (13), (14), (17) and (18)
5. Update $R(p_{n,k}, p_{n,i}, p_{n,l}, p_{n,j})$ according to (22)
6. Update $\psi^{[t+1]}$ and $\phi^{[t+1]}$ according to Lemma1
7. **if** $\gamma^{[t+1]} - \gamma^{[t]} \leq \delta$ **then**
8. Exit
9. **else**
10. $t \leftarrow t + 1$ and repeat step 2
11. **end if**

If $(p^{(',w_n)}, R_2^{(',w_n)}, p^{('',w_n)}, R_2^{('',w_n)})$ denote optimum solution for total powers and data rates corresponding to a particular λ_n and w, then optimum solution of the problem with Lagrange Multipliers $(\lambda_n', \lambda_n'')$ and weights (w_1, w_2) implies that $\lambda_n' p' + \lambda_n'' p'' < \lambda_n' p^{(',w,\lambda_n)} + \lambda_n'' p^{('',w,\lambda_n)}$ and $w_1 R_2' + w_2 R_2'' < w_1 R_2^{(',w,\lambda_n)} + w_2 R_2^{('',w,\lambda_n)}$.

We need to adjust λ_n and w in order to satisfy the following constraints: $p^{(',w,\lambda_n)} = p^{(',max)}, p^{('',w,\lambda_n)} = p^{('',max)}, R_2^{(',w,\lambda_n)} \geq R_2^{(',th)}$ and $R_2^{('',w,\lambda_n)} \geq R_2^{('',th)}$, so that weighted power sum and weighted data rate sum become higher than any other tentative set of consideration either in the colored triangle or rectangle region.

In the consideration of two optimum solutions such as $(p^{(',w_a,\lambda_n^a)}, R_2^{(',w_a,\lambda_n^a)}, p^{('',w_a,\lambda_n^a)}, R_2^{('',w_a,\lambda_n^a)})$ and $(p^{(',w_b,\lambda_n^b)}, R_2^{(',w_b,\lambda_n^b)}, p^{('',w_b,\lambda_n^b)}, R_2^{('',w_b,\lambda_n^b)})$ for (w_a, λ_n^a) and (w_b, λ_n^b) respectively, the optimum solution $(p^{(',w_a,\lambda_n^a)}, R_2^{(',w_a,\lambda_n^a)}, p^{('',w_a,\lambda_n^a)}, R_2^{('',w_a,\lambda_n^a)})$ for (w_a, λ_n^a) turns into the following expression,

$$\begin{aligned} &w_a' R_2^{(',w_b,\lambda_n^b)} + w_a'' R_2^{('',w_b\lambda_n^b)} - \lambda_n^{(',a)} p^{(',w_b,\lambda_n^b)} \\ &\quad - \lambda_n^{('',a)} p^{('',w_b,\lambda_n^b)} \leq w_a' R_2^{(',w_a,\lambda_n^a)} + w_a'' R_2^{('',w_a\lambda_n^a)} \\ &\quad - \lambda_n^{(',a)} p^{(',w_a,\lambda_n^a)} - \lambda_n^{('',a)} p^{('',w_a,\lambda_n^a)}, \end{aligned} \tag{35}$$

As the part of (35) is on the right certainly utilize the condition that optimizes the Lagrangian for $(w_a', \lambda_n^{(',a)}, w_a'', \lambda_n^{('',a)})$, no other conditions corresponding to $(p^{(',w_b,\lambda_n^b)}, R_2^{(',w_b,\lambda_n^b)}, p^{(',w_b,\lambda_n^b)}, R_2^{('',w_b,\lambda_n^b)})$ turn into a higher value for the Lagrangian.

Based on the same statement, the optimum solution $(p^{(',w_b,\lambda_n^b)}, R_2^{(',w_b,\lambda_n^b)}, p^{('',w_b,\lambda_n^b)}, R_2^{('',w_b,\lambda_n^b)})$ for (w_b, λ_n^b) can lead into the following expression,

$$\begin{aligned} &w_b' R_2^{(',w_a,\lambda_n^a)} + w_b'' R_2^{('' w_a\lambda_n^a)} - \lambda_n^{(',b)} p^{(',w_a,\lambda_n^a)} \\ &\quad - \lambda_n^{('',b)} p^{('',w_a,\lambda_n^a)} \leq w_b' R_2^{(',w_b,\lambda_n^b)} + w_b'' R_2^{('' w_b\lambda_n^b)} \\ &\quad - \lambda_n^{(',b)} p^{(',w_b,\lambda_n^b)} - \lambda_n^{('',b)} p^{('',w_b,\lambda_n^b)}. \end{aligned} \tag{36}$$

By adding (35) and (36), we get

$$\begin{aligned} &-(w_b' - w_a')(R_2^{(',w_b,\lambda_n^b)} - R_2^{(',w_a,\lambda_n^a)}) \\ &\quad - (w_b'' - w_a'')(R_2^{('',w_b,\lambda_n^b)} - R_2^{('',w_a,\lambda_n^a)}) \\ &\quad + (\lambda_n^{(',b)} - \lambda_n^{(',a)})(p^{(',w_b,\lambda_n^b)} - p^{(',w_a,\lambda_n^a)}) \\ &\quad + (\lambda_n^{('',b)} - \lambda_n^{('',a)})(p^{('',w_b,\lambda_n^b)} - p^{('',w_a,\lambda_n^a)}) \leq 0. \end{aligned} \tag{37}$$

Further, (37) for a pair of users can be re-expressed for N-user as

$$\begin{bmatrix} -(\Delta w)^T & (\Delta\lambda_n)^T \end{bmatrix} \begin{bmatrix} \Delta R \\ \Delta p \end{bmatrix} \leq 0, \tag{38}$$

where $\Delta w = [\Delta w', \Delta w'' \cdots \Delta w^N]^T$, $\Delta\lambda_n = [\Delta\lambda_n', \Delta\lambda_n'' \cdots \Delta\lambda_n^N]^T$, $\Delta R = [\Delta R', \Delta R'' \cdots \Delta R^N]^T$, and $\Delta p = [\Delta p', \Delta p'' \cdots \Delta p^N]^T$ denote vectors for the corresponding weights, Lagrange multipliers, data rates and powers.

Based on the condition of w and λ_n, (38) can be classified into the following cases:

$$\text{At fixed } w, \quad (\Delta\lambda_n)^T \Delta p \leq 0 \Big|_{\Delta w=0}, \tag{39}$$

$$\text{At fixed } \lambda_n, \quad (\Delta w)^T \Delta R \geq 0 \Big|_{\Delta\lambda_n=0}. \tag{40}$$

(38) is a useful expression for establishing a operation to determine w and λ_n that carry out the constraints. Due to negative product of $\Delta\lambda_n$ and Δp, $\Delta\lambda_n$ for the required Δp should be somewhere around the colored triangle plane on the opposite side of the Δp vector. With the regulation of λ_n by varying the $\Delta\lambda_n$ vector, (39) promises with certainty to achieve very near to $(p^{',max}, p^{'',max})$ provided that $\Delta\lambda_n$ is not very high. It is illustrated in Figure 2 that the $\Delta\lambda_n$ drives $(p^{',w,\lambda_n}, p^{'',w,\lambda_n})$ to the next point on the inner side of the circle.

Hence, the Lagrange multipliers' solutions can then iteratively express by applying the gradient descent method as below,

$$\begin{cases} \lambda_n^{1[t+1]} = \left[\lambda_n^{1[t]} + \varpi^{[t]}(\sum_{n=1}^{N_{sc}} p_{n,k} - p_{max1})\right]^+, \\ \lambda_n^{2[t+1]} = \left[\lambda_n^{2[t]} + \varpi^{[t]}(\sum_{n=1}^{N_{sc}} p_{n,i} - p_{max2})\right]^+, \\ \lambda_n^{3[t+1]} = \left[\lambda_n^{3[t]} + \varpi^{[t]}(\sum_{n=1}^{N_{sc}} p_{n,l} - p_{max3})\right]^+, \\ \lambda_n^{4[t+1]} = \left[\lambda_n^{4[t]} + \varpi^{[t]}(\sum_{n=1}^{N_{sc}} p_{n,j} - p_{max4})\right]^+, \end{cases} \tag{41}$$

where $\varpi^{[t]}$ stands for a sequence of scalar step size at t^{th} iteration and $[Z]^+ = \max(0, Z)$[4].

Since MC-ILBCS algorithm can only achieve a lower-bound solution that is suboptimal, we propose another algorithm based on sub-channel iterative Lagrange multipliers

[4]For a real number Z, $[Z]^- = \max(-Z, 0) = -\min(0, Z)$

Algorithm 2 Sub-Channel Iterative Lagrange Multipliers Search

1. Initialize $t = 1$ $w_{min} = 0$, $w_{max} = 1$, $\lambda^1_{n(min)} = 0$, $\lambda^1_{n(max)} = 1$, $\lambda^2_{n(min)} = 0$, $\lambda^2_{n(max)} = 1$, $\lambda^3_{n(min)} = 0$, $\lambda^3_{n(max)} = 1$, $\lambda^4_{n(min)} = 0$, $\lambda^4_{n(max)} = 1$, $\varpi = 1$.
2. **for** all sub-channels n **do**
3. **while** $\gamma_n - R_2^{th} > \varsigma$ **do**
4. $w = \frac{w_{min}+w_{max}}{2}$
5. **while** $\sum_{n=1}^{N_{sc}} p_{n,k} - p_{max1} > \varsigma$ **do**
6. $\lambda^1_n = \frac{\lambda^1_{n(min)}+\lambda^1_{n(max)}}{2}$
7. $p_{n,k} \leftarrow \arg\max_{\{\bar{p}_{n,k},\bar{p}_{n,i},\bar{p}_{n,l},\bar{p}_{n,j}\}} L$ $(\tilde{p}, \lambda_n^{1[t]}, \lambda_n^{2[t]}, \lambda_n^{3[t]}, \lambda_n^{4[t]})$
8. *if* $\sum_{n=1}^{N_{sc}} p_{n,k} > p_{max1}$ **then**
9. $\lambda^1_{n(min)} = \lambda^1_n$
10. **else**
11. $\lambda^1_{n(max)} = \lambda^1_n$
12. **end if**
13. **end while**
14. **while** $\sum_{n=1}^{N_{sc}} p_{n,i} - p_{max2} > \varsigma$ **do**
15. $\lambda^2_n = \frac{\lambda^2_{n(min)}+\lambda^2_{n(max)}}{2}$
16. $p_{n,i} \leftarrow \arg\max_{\{\bar{p}_{n,k},\bar{p}_{n,i},\bar{p}_{n,l},\bar{p}_{n,j}\}} L$ $(\tilde{p}, \lambda_n^{1[t]}, \lambda_n^{2[t]}, \lambda_n^{3[t]}, \lambda_n^{4[t]})$
17. *if* $\sum_{n=1}^{N_{sc}} p_{n,i} > p_{max2}$ **then**
18. $\lambda^2_{n(min)} = \lambda^2_n$
19. **else**
20. $\lambda^2_{n(max)} = \lambda^2_n$
21. **end if**
22. **end while**
23. **while** $\sum_{n=1}^{N_{sc}} p_{n,l} - p_{max3} > \varsigma$ **do**
24. $\lambda^3_n = \frac{\lambda^3_{n(min)}+\lambda^3_{n(max)}}{2}$
25. $p_{n,l} \leftarrow \arg\max_{\{\bar{p}_{n,k},\bar{p}_{n,i},\bar{p}_{n,l},\bar{p}_{n,j}\}} L$ $(\tilde{p}, \lambda_n^{1[t]}, \lambda_n^{2[t]}, \lambda_n^{3[t]}, \lambda_n^{4[t]})$
26. *if* $\sum_{n=1}^{N_{sc}} p_{n,l} > p_{max3}$ **then**
27. $\lambda^3_{n(min)} = \lambda^3_n$
28. **else**
29. $\lambda^3_{n(max)} = \lambda^3_n$
30. **end if**
31. **end while**
32. **while** $\sum_{n=1}^{N_{sc}} \sum_{n=1}^{N_{sc}} p_{n,j} - p_{max4} > \varsigma$ **do**
33. $\lambda^4_n = \frac{\lambda^4_{n(min)}+\lambda^4_{n(max)}}{2}$
34. $p_{n,j} \leftarrow \arg\max_{\{\bar{p}_{n,k},\bar{p}_{n,i},\bar{p}_{n,l},\bar{p}_{n,j}\}} L$ $(\tilde{p}, \lambda_n^{1[t]}, \lambda_n^{2[t]}, \lambda_n^{3[t]}, \lambda_n^{4[t]})$
35. *if* $\sum_{n=1}^{N_{sc}} p_{n,j} > p_{max4}$ **then**
36. $\lambda^4_{n(min)} = \lambda^4_n$
37. **else**
38. $\lambda^4_{n(max)} = \lambda^4_n$
39. **end if**
40. **end while**

search. This algorithm achieves an optimal solution, but it comes with additional computational complexity.

Algorithm 2 *(Continued.)* Sub-Channel Iterative Lagrange Multipliers Search

41. *if* $\gamma_n > R_2^{th}$ **then**
42. $w_{max} = w$
43. else
44. $w_{min} = w$
45. **end if**
46. **end while**
47. **while** $A >$deviation **do**
48. λ_n=optimum λ_n
49. **while** distance $\leq$ preceding A **do**
50. (preceding A) $= A$
51. $\varpi = \varpi \times 2$
52. $\Delta\lambda_n = -\varpi(p_{max} - p_{\lambda_n})$
53. Compute (31) by exhaustive search.
54. $A = ||p_{max} - p_{\lambda_n+\Delta\lambda_n}||$
55. **end while**
56. **end while**
57. **end for**

TABLE 2. Complexity analysis.

Algorithm	Complexity (Order)	Operations in each cycle	Run time (Sec)	Performance
Algorithm 1	$O(N_{sc}N)$	$79.8N_{sc}N$	15	Suboptimal
Algorithm 2	$O(N_{sc}N)$	$N_{sc}N(b_{n(max)}+1)^N(39.9)^{2N}$	47	Optimal

B. COMPUTATIONAL COMPLEXITY ANALYSIS

The operation of algorithm 1 includes an outer cycle that iterates through computation and update of (28), (33), (13), (14), (17), (22) and Lemma 1, and an inner loop that regulates the RSS associated to a user until the set data rate is reached. The complexity associated with inner loop due to optimal water level search and bitloading is $2N_{sc}$. Including $\log_2(\frac{1}{\eta_\lambda})$ iterations for bisection search, the iterations for all the users, and the iteration of the entire process, the overall complexity of algorithm 1 is becoming: $2N_{sc}N\log_2(\frac{1}{\eta_\lambda})$.

Algorithm 2 starts by searching upper and lower bounds on λ^1_n, λ^2_n, λ^3_n, λ^4_n, that can be stored to $\lambda^1_{n(max)}$, $\lambda^2_{n(max)}$, $\lambda^3_{n(max)}$, $\lambda^4_{n(max)}$ and $\lambda^1_{n(min)}$, $\lambda^2_{n(min)}$, $\lambda^3_{n(min)}$, $\lambda^4_{n(min)}$, respectively. The leading complexity takes place in the outer loops of the algorithm 2, where bisection is performed on λ^1_n, λ^2_n, λ^3_n, λ^4_n subject to power constraints on the users should satisfy.

We assume that the precision of η_λ is the minimum requirement to achieve the target data rate. Therefore, this needs $\log_2(\frac{1}{\eta_\lambda})$ iterations to optimize each Lagrange multiplier, which results in $\log_2(\frac{1}{\eta_\lambda})^4$ iterations during bisection search. In order to have accuracy of about less than 1% on both w and λ_n, we require total of $\log_2(\frac{1}{\eta_\lambda})^8$ iterations with $\eta_\lambda = 10^{-12}$. In the discrete bit loading with N_{sc} sub-channels for N users, optimization function requires $N_{sc}N(b_{n(max)}+1)^N$ evaluations where $b_n \triangleq [b_n^1, \cdots, b_n^N]^T$, $N = N_{FU} + N_{MU}$.

The total complexity associated with algorithm 2 is then: $N_{sc}N(b_{n(max)}+1)^N \log_2(\frac{1}{\eta_\lambda})^{2N}$.

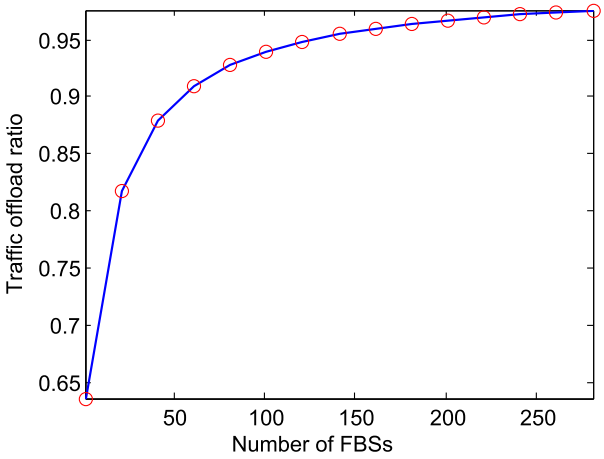

FIGURE 3. Macrocell traffic offload ratio vs. number of FBS in the system.

TABLE 3. Simulation setup.

Parameter	Value
Outer radius of macrocell	3000 m
Interference protection radius of macrocell	600 m
Interference protection radius of femto transmitter	240 m
Ambient temperature	250 kelvins
Channel coherence	64 blocks
Channel type	Rician fading
Channel Bandwidth	100 MHz
No of sub-channels per sub-band	10
Achievable symbol error probability	10^{-12}
Noise margin	4 dB
Optimum bit loading	32 bits
User's velocity	20 m/s
Data rate	133 Mbps
Wavelength	0.15 m
Doppler frequency	133 Mbps
Normalized doppler frequency	10^{-6}

IV. NUMERICAL RESULTS AND DISCUSSION

In this section, numerical results are provided for the proposed power control schemes. Since the channel model studied is novel, only a limited performance comparison with state of the art research can be done, where the CDF of SE for the scheme by [57] and this paper's proposed schemes: algorithms 1 and 2 are compared. However, a comprehensive performance evaluation of proposed schemes with state of the art is an interesting study topic for a future paper.

System performance has been evaluated based on the derivations in sections II and III. The channel characteristics based upon the corresponding transmission distance have been computed according to the following assumptions. The path-loss in dB corresponding to $d_{n,i,k}$ is calculated as [65]: $L(d_{n,i,k}) = [44.9 - 6.55\log_{10}(h_{BS})]\log_{10}(d_{n,i,k}) + 34.46 + 5.83\log_{10}(h_{BS}) + 23\log_{10}(\frac{f_c}{5}) + e_{n,i,k}\varphi_{n,i,k}$, where h_{BS} is the BS height that is selected as 30 m and 10 m for MBS and FBS, respectively; carrier frequency $f_c = 2.5$ GHz; additionally, $e_{n,i,k}$ indicates the number of walls and $\varphi_{n,i,k}$ indicates the wall penetration loss. It is assumed that $\varphi_{n,i,k}$=5 dB for $e_{n,i,k}$=1 and $\varphi_{n,i,k}$=12 dB for $e_{n,i,k}$=2.

Figure 3 shows the macrocell traffic offload ratio versus number of FBS deployed in the system. It can be seen that as the number of FBS increases the offload ratio increases and with a very dense deployment of FBS it is possible to completely offload macrocell traffic to FBSs. This can be used for ultra-high speed and reliable communications in future wireless networks. When the number of FBSs is between 1 to 100, the increase at offload ratio is very high and this increase slows down when number of FBSs are more than 100. This shows that the addition of even small number of FBSs initially provides significant gain.

Figure 4(a)-(c) shows the upper bound on the number of admitted secondary users versus the outage probability threshold, SINR and channel gain for different values of spectral efficiency. Figure 4(a) shows that there is a linear relationship between the upper bound on the number of admitted secondary users and the outage probability threshold. Also, as the spectral efficiency increases, the number of admitted secondary users increases. In figure 4(b), the relationship between the upper bound on the number of admitted secondary users and SINR is shown to be logarithmic, where for a given spectral efficiency, most of the increase is obtained at the low SINR regime, between 1-5 dB. Figure 4(c) shows that there is an exponential relationship between channel gain and the upper bound on the number of admitted secondary users. Also the number of admitted secondary users increases as the spectral efficiency increases. It is evident from above discussion that channel gain has the most effect on increasing the number of admitted secondary users, accordingly engineers that aim to increase this value shall focus on improving channel gain.

Figure 5 shows the CDF of SE for various FFR values, where UL T_x power per user = {0.1, 0.5} W and the number of FBSs = 16. It can be seen from the figure that for both UL T_x power scenarios the performance increases as the FFR value increases from 1 to 3 and then it degrades as the FFR = 4. Thus, the optimal reuse factor is shown to be 3; this is in accordance with the literature. Performance improvement due to varying the FFR value demonstrates the effectiveness of FFR technique for interference management for cell-edge users. Further, the increase of UL T_x power per user significantly improves the performance where the performance gain stays constant for considered FFR values.

Figure 6 shows the CDF of SE for the scheme by [57] and this paper's proposed schemes: algorithms 1 and 2. The scheme by [57] is based on cognitive radio technology and comprised of two steps that are channel sensing with fractional frequency reuse and resource scheduling to manage heterogeneous interference problem. Proposed algorithm 1 uses multi-channel iterative lower-bound coefficients search and algorithm 2 employs sub-channel iterative Lagrange multipliers search, where the details are given in

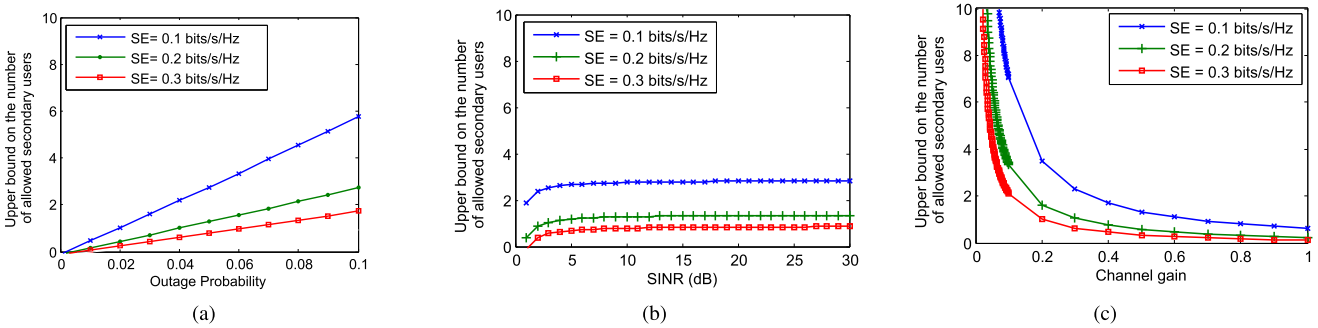

FIGURE 4. The upper bound on the number of admitted secondary users versus (a) outage probability, (b) SINR and (c) channel gain.

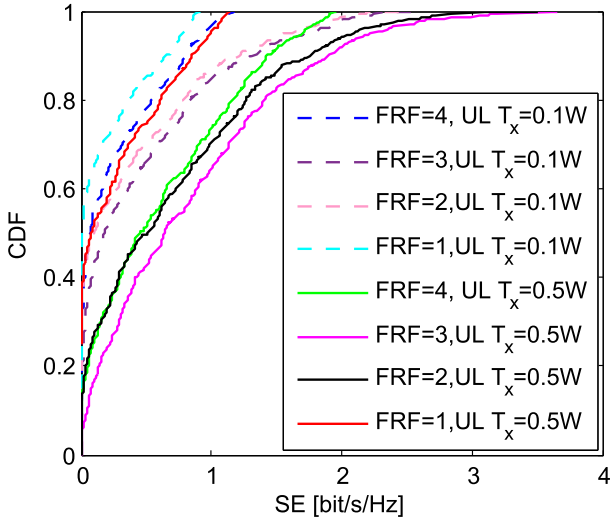

FIGURE 5. CDF of SE for various FRFs, where UL T_X power per user = 0.1 and 0.5 W and the number of FBSs = 16.

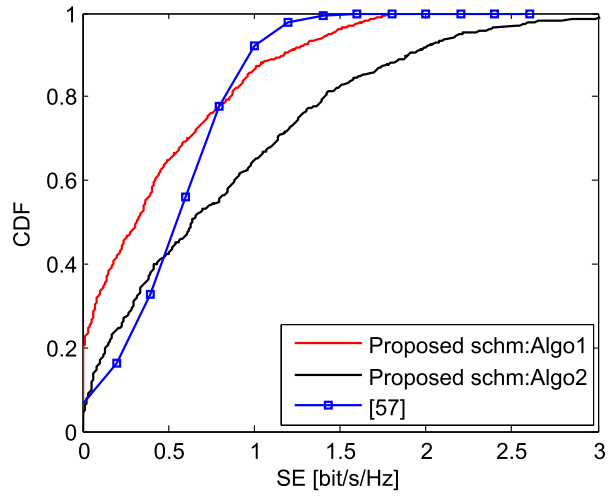

FIGURE 6. CDF of SE for optimal FRF, where UL T_X power per user = 0.5 W and the number of FBSs = 16.

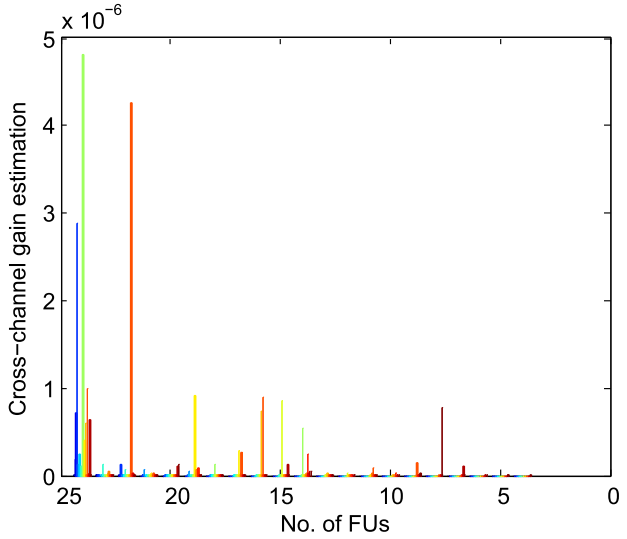

FIGURE 7. Cross-channel gain estimation versus number of femto users.

section III-A. It can be seen from the figure that the scheme by [57] is very effective at mitigating severe interference since it achieves the lowest percentage of users achieving SE between 0 to 0.5 bits/s/Hz compared to algorithms 1 and 2. However, for the rest of the SE region considered in the simulations, the proposed scheme with algorithm 2 outperforms the other scheme by [57] and the algorithm 1. Thus, algorithm 2 is a good candidate for next generation ultra-high speed communications where high SE regions are interested. Further, it should be noted from table 2 that algorithm 2 has a higher computational complexity compared to algorithm 1. For systems with limited computation power and time requirements, there can be a performance-complexity trade-off.

Figure 7 shows the cross-channel gain estimation versus number of FUs. It can be seen from the figure that as the number of FUs decreases, the cross-channel gain decreases. This is due to a smaller number of users distributed over the geographical area and accordingly a reduced multi-user gain. Cross-channel gain is especially important for mobile applications that may require frequent vertical handovers. Having high cross-channel gain improves reliability for these applications and thus high user-density systems are favorable for their deployment.

V. CONCLUSION

This paper proposes a channel model for mobile mmWave massive MIMO based two-tier networks. The user mobility introduces a variable number of clusters and rays within each cluster at the mmWave channel. These properties of the mmWave channel have not been studied for two-tier networks. Studying this new channel model and power control schemes have been proposed. A flexible power control scheme is given that maximizes the total system capacity. It uses a multi-channel iterative lower-bound coefficients search algorithm to find the optimum solution. Number of SUs admitted to the system, SE, cross-channel gain estimation and macrocell traffic offload ratio metrics are investigated and discussed.

Finally, it should be noted that the proposed channel model and schemes can be extended to multi-tier networks where the number of tiers is larger than two. As the first study of the channel model and proposed schemes in a multi-tier network architecture, this paper considers a two-tier case for the algorithms and mathematical derivations to be easy to follow. Lack of available data and priori research studies on the proposed channel model are limitations of this study. Authors encourage researchers to use this model at their studies to increase the availability of data and provide opportunity for performance comparison between different proposals.

REFERENCES

[1] F. E. Idachaba, "5G networks: Open network architecture and densification strategies for beyond 1000x network capacity increase," in *Proc. Future Technol. Conf. (FTC)*, Dec. 2016, pp. 1265–1269.

[2] P. Ji, X. Jia, Y. Lu, H. Hu, and Y. Ouyang, "Multi-UAV assisted multi-tier millimeter-wave cellular networks for hotspots with 2-tier and 4-tier network association," *IEEE Access*, vol. 8, pp. 158972–158995, 2020.

[3] P. D. Mankar, G. Das, and S. S. Pathak, "Coverage analysis of two-tier HetNets for co-channel, orthogonal, and partial spectrum sharing under fractional load conditions," *IEEE Trans. Veh. Technol.*, vol. 66, no. 8, pp. 7149–7163, Aug. 2017.

[4] P.-Y. Kong and A. Sluzek, "Average packet delay analysis for a mobile user in a two-tier heterogeneous cellular network," *IEEE Syst. J.*, vol. 11, no. 4, pp. 2726–2736, Dec. 2017.

[5] V. Chandrasekhar, J. G. Andrews, and A. Gatherer, "Femtocell networks: A survey," *IEEE Commun. Mag.*, vol. 46, no. 9, pp. 59–67, Sep. 2008.

[6] W. Wang, G. Yu, and A. Huang, "Cognitive radio enhanced interference coordination for femtocell networks," *IEEE Commun. Mag.*, vol. 51, no. 6, pp. 37–43, Jun. 2013.

[7] S. M. Cheng, S. Y. Lien, F. S. Chu, and K. C. Chen, "On exploiting cognitive radio to mitigate interference in macro/femto heterogeneous networks," *IEEE Wireless Commun.*, vol. 18, no. 3, pp. 40–47, Jun. 2011.

[8] Y.-Y. Li and E. S. Sousa, "Cognitive femtocell: A cost-effective approach towards 4G autonomous infrastructure networks," *Wireless Pers. Commun.*, vol. 64, no. 1, pp. 65–78, May 2012.

[9] Q. Liu, T. Han, N. Ansari, and G. Wu, "On designing energy-efficient heterogeneous cloud radio access networks," *IEEE Trans. Green Commun. Netw.*, vol. 2, no. 3, pp. 721–734, Sep. 2018.

[10] V. Chandrasekhar and J. G. Andrews, "Spectrum allocation in tiered cellular networks," *IEEE Trans. Commun.*, vol. 57, no. 10, pp. 3059–3068, Oct. 2009.

[11] H. Zhang, C. Jiang, N. C. Beaulieu, X. Chu, X. Wen, and M. Tao, "Resource allocation in spectrum-sharing OFDMA femtocells with heterogeneous services," *IEEE Trans. Commun.*, vol. 62, no. 7, pp. 2366–2377, Jul. 2014.

[12] H. Zhu and J. Wang, "Radio resource allocation in multiuser distributed antenna systems," *IEEE J. Sel. Areas Commun.*, vol. 31, no. 10, pp. 2058–2066, Oct. 2013.

[13] U. Kozat and L. Tassiulas, "Throughput capacity of random ad hoc networks with infrastructure support," in *Proc. MobiCom*, 2003, pp. 55–65.

[14] R. Xie, F. R. Yu, H. Ji, and Y. Li, "Energy-efficient resource allocation for heterogeneous cognitive radio networks with femtocells," *IEEE Trans. Wireless Commun.*, vol. 11, no. 11, pp. 3910–3920, Nov. 2012.

[15] Z. Cheng, M. Tao, and P.-Y. Kam, "Channel path identification in mmWave systems with large-scale antenna arrays," *IEEE Trans. Commun.*, vol. 68, no. 9, pp. 5549–5562, Sep. 2020.

[16] H. Xie, F. Gao, and S. Jin, "An overview of low-rank channel estimation for massive MIMO systems," *IEEE Access*, vol. 4, pp. 7313–7321, 2016.

[17] G. R. Maccartney, T. S. Rappaport, M. K. Samimi, and S. Sun, "Millimeter-wave omnidirectional path loss data for small cell 5G channel modeling," *IEEE Access*, vol. 3, pp. 1573–1580, 2015.

[18] G. R. Maccartney, T. S. Rappaport, S. Sun, and S. Deng, "Indoor office wideband millimeter-wave propagation measurements and channel models at 28 and 73 GHz for ultra-dense 5G wireless networks," *IEEE Access*, vol. 3, pp. 2388–2424, 2015.

[19] C. Gustafson, K. Haneda, S. Wyne, and F. Tufvesson, "On mm-wave multipath clustering and channel modeling," *IEEE Trans. Antennas Propag.*, vol. 62, no. 3, pp. 1445–1455, Mar. 2014.

[20] S. Sangodoyin, V. Kristem, A. F. Molisch, R. He, F. Tufvesson, and H. M. Behairy, "Statistical modeling of ultrawideband MIMO propagation channel in a warehouse environment," *IEEE Trans. Antennas Propag.*, vol. 64, no. 9, pp. 4049–4063, Sep. 2016.

[21] J. Chen, X. Yin, X. Cai, and S. Wang, "Measurement-based massive MIMO channel modeling for outdoor LoS and NLoS environments," *IEEE Access*, vol. 5, pp. 2126–2140, 2017.

[22] X. Cai, G. Zhang, C. Zhang, W. Fan, J. Li, and G. F. Pedersen, "Dynamic channel modeling for indoor millimeter-wave propagation channels based on measurements," *IEEE Trans. Commun.*, vol. 68, no. 9, pp. 5878–5891, Sep. 2020.

[23] M. Zhou, H. Li, N. Zhao, S. Zhang, and F. R. Yu, "Feasibility analysis and clustering for interference alignment in full-duplex-based small cell networks," *IEEE Trans. Commun.*, vol. 67, no. 1, pp. 807–819, Jan. 2019.

[24] X. Zhao and D. Pompili, "Multi-cell interference management scheme for next-generation cellular networks," *IEEE Trans. Commun.*, vol. 68, no. 2, pp. 1200–1212, Feb. 2020.

[25] M. D. Yacoub, "The $\alpha - \eta - \kappa - \mu$ fading model," *IEEE Trans. Antennas Propag.*, vol. 64, no. 8, pp. 3597–3610, Aug. 2016.

[26] T. R. R. Marins, A. A. dos Anjos, V. M. R. Penarrocha, L. Rubio, J. Reig, R. A. A. de Souza, and M. D. Yacoub, "Fading evaluation in the mm-wave band," *IEEE Trans. Commun.*, vol. 67, no. 12, pp. 8725–8738, Dec. 2019.

[27] T. Hwang, C. Yang, G. Wu, S. Li, and G. Y. Li, "OFDM and its wireless applications: A survey," *IEEE Trans. Veh. Technol.*, vol. 58, no. 4, pp. 1673–1694, May 2009.

[28] W. Guo, W. Zhang, P. Mu, and F. Gao, "High-mobility OFDM downlink transmission with large-scale antenna array," *IEEE Trans. Veh. Technol.*, vol. 66, no. 9, pp. 8600–8604, Sep. 2017.

[29] Y. Ge, W. Zhang, and F. Gao, "High-mobility OFDM downlink transmission with partly calibrated subarray-based massive uniform linear array," in *Proc. IEEE 85th Veh. Technol. Conf. (VTC Spring)*, Jun. 2017, pp. 1–6.

[30] Y. Ge, W. Zhang, F. Gao, and H. Minn, "Angle-domain approach for parameter estimation in high-mobility OFDM with fully/partly calibrated massive ULA," *IEEE Trans. Wireless Commun.*, vol. 18, no. 1, pp. 591–607, Jan. 2019.

[31] W. Guo, W. Zhang, P. Mu, F. Gao, and B. Yao, "Angle-domain Doppler pre-compensation for high-mobility OFDM uplink with massive ULA," in *Proc. IEEE Global Commun. Conf. (GLOBECOM)*, Dec. 2017, pp. 1–6.

[32] W. Guo, W. Zhang, P. Mu, F. Gao, and H. Lin, "High-mobility wideband massive MIMO communications: Doppler compensation, analysis and scaling laws," *IEEE Trans. Wireless Commun.*, vol. 18, no. 6, pp. 3177–3191, Jun. 2019.

[33] Y. Ge, W. Zhang, F. Gao, S. Zhang, and X. Ma, "High-mobility massive MIMO with beamforming network optimization: Doppler spread analysis and scaling law," *IEEE J. Sel. Areas Commun.*, vol. 38, no. 12, pp. 2889–2902, Dec. 2020.

[34] J. Huang, C.-X. Wang, H. Chang, J. Sun, and X. Gao, "Multi-frequency multi-scenario millimeter wave MIMO channel measurements and modeling for B5G wireless communication systems," *IEEE J. Sel. Areas Commun.*, vol. 38, no. 9, pp. 2010–2025, Sep. 2020.

[35] J. Zhang, H. Du, P. Zhang, J. Cheng, and L. Yang, "Performance analysis of 5G mobile relay systems for high-speed trains," *IEEE J. Sel. Areas Commun.*, vol. 38, no. 12, pp. 2760–2772, Dec. 2020.

[36] B. Luo, P. L. Yeoh, and B. S. Krongold, "Optimal co-phasing power allocation and capacity of coordinated OFDM transmission with total and individual power constraints," *IEEE Trans. Commun.*, vol. 67, no. 10, pp. 7103–7113, Oct. 2019.
[37] M. Sheng, L. Wang, X. Wang, Y. Zhang, C. Xu, and J. Li, "Energy efficient beamforming in MISO heterogeneous cellular networks with wireless information and power transfer," *IEEE J. Sel. Areas Commun.*, vol. 34, no. 4, pp. 954–968, Apr. 2016.
[38] J. Ghosh, V. Sharma, H. Haci, S. Singh, and I.-H. Ra, "Performance investigation of NOMA versus OMA techniques for mmWave massive MIMO communications," *IEEE Access*, vol. 9, pp. 125300–125308, 2021.
[39] F. Fang, G. Ye, H. Zhang, J. Cheng, and V. C. M. Leung, "Energy-efficient joint user association and power allocation in a heterogeneous network," *IEEE Trans. Wireless Commun.*, vol. 19, no. 11, pp. 7008–7020, Nov. 2020.
[40] A. M. Abdelhady, O. Amin, and M.-S. Alouini, "Energy-efficient resource allocation for phantom cellular networks with imperfect CSI," *IEEE Trans. Wireless Commun.*, vol. 16, no. 6, pp. 3799–3813, Jun. 2017.
[41] N.-T. Le, L.-N. Tran, Q.-D. Vu, and D. Jayalath, "Energy-efficient resource allocation for OFDMA heterogeneous networks," *IEEE Trans. Commun.*, vol. 67, no. 10, pp. 7043–7057, Oct. 2019.
[42] S. A. R. Naqvi, H. Pervaiz, S. A. Hassan, L. Musavian, Q. Ni, M. A. Imran, X. Ge, and R. Tafazolli, "Energy-aware radio resource management in D2D-enabled multi-tier HetNets," *IEEE Access*, vol. 6, pp. 16610–16622, 2018.
[43] W. Liu, K.-K. Wong, S. Jin, and X. You, "A data-aided channel estimation scheme for decoupled systems in heterogeneous networks," *IEEE Trans. Wireless Commun.*, vol. 17, no. 8, pp. 4987–5000, Aug. 2018.
[44] W. Liu, S. Jin, M. Matthaiou, and X.-H. You, "Transmission scheme and performance analysis of multi-cell decoupled heterogeneous networks," *IEEE Trans. Commun.*, vol. 68, no. 7, pp. 4423–4436, Jul. 2020.
[45] R. Amiri, M. A. Almasi, J. G. Andrews, and H. Mehrpouyan, "Reinforcement learning for self organization and power control of two-tier heterogeneous networks," *IEEE Trans. Wireless Commun.*, vol. 18, no. 8, pp. 3933–3947, Aug. 2019.
[46] L. Xiao, H. Zhang, Y. Xiao, X. Wan, S. Liu, L.-C. Wang, and H. V. Poor, "Reinforcement learning-based downlink interference control for ultra-dense small cells," *IEEE Trans. Wireless Commun.*, vol. 19, no. 1, pp. 423–434, Jan. 2020.
[47] P. Lohan and D. Mishra, "Utility-aware optimal resource allocation protocol for UAV-assisted small cells with heterogeneous coverage demands," *IEEE Trans. Wireless Commun.*, vol. 19, no. 2, pp. 1221–1236, Feb. 2020.
[48] R. Yin, S. Liu, G. Yu, Y. Zhang, and Q. Chen, "Semi-distributed joint power and spectrum allocation for LAA based small cell networks," *IEEE Trans. Wireless Commun.*, vol. 19, no. 6, pp. 4141–4153, Jun. 2020.
[49] G. Chandrasekaran, P. R. Karthikeyan, N. S. Kumar, and V. Kumarasamy, "Test scheduling of system-on-chip using dragonfly and ant lion optimization algorithms," *J. Intell. Fuzzy Syst.*, vol. 40, no. 3, pp. 4905–4917, Mar. 2021.
[50] G. Chandrasekaran, S. Periyasamy, and K. P. Rajamanickam, "Minimization of test time in system on chip using artificial intelligence-based test scheduling techniques," *Neural Comput. Appl.*, vol. 32, no. 9, pp. 5303–5312, May 2020.
[51] G. Chandrasekaran, S. Periyasamy, and P. R. Karthikeyan, "Test scheduling for system on chip using modified firefly and modified ABC algorithms," *Social Netw. Appl. Sci.*, vol. 1, no. 9, p. 1079, Sep. 2019.
[52] J. Ghosh, H. Zhu, and H. Haci, "A novel channel model and optimal beam tracking schemes for mobile millimeter-wave massive MIMO communications," *IEEE Trans. Veh. Technol.*, vol. 70, no. 7, pp. 7205–7210, Jul. 2021.
[53] S. N. Ch iu, D. Stoyan, W. S. Kendall, and J. Mecke, *Stochastic Geometry and Its Applications*. Hoboken, NJ, USA: Wiley, 2013.
[54] M. Shafi, J. Zhang, H. Tataria, A. F. Molisch, S. Sun, T. S. Rappaport, F. Tufvesson, S. Wu, and K. Kitao, "Microwave vs. millimeter-wave propagation channels: Key differences and impact on 5G cellular systems," *IEEE Commun. Mag.*, vol. 56, no. 12, pp. 14–20, Dec. 2018.
[55] T. S. Rappaport, S. Sun, R. Mayzus, H. Zhao, Y. Azar, K. Wang, G. N. Wong, J. K. Schulz, M. Samimi, and F. Gutierrez, "Millimeter wave mobile communications for 5G cellular: It will work!" *IEEE Access*, vol. 1, pp. 335–349, 2013.
[56] J. Ghosh, "A trade-off between energy efficiency and spectral efficiency in macro-femtocell networks," *IEEE Trans. Veh. Technol.*, vol. 69, no. 10, pp. 10914–10924, Oct. 2020.
[57] D. C. Oh and Y. H. Lee, "Cognitive radio based resource allocation in femto-cell," *J. Commn. Net.*, vol. 14, no. 3, pp. 252–256, 2012.
[58] T. D. Novlan, R. K. Ganti, A. Ghosh, and J. G. Andrews, "Analytical evaluation of fractional frequency reuse for heterogeneous cellular networks," *IEEE Trans. Commun.*, vol. 60, no. 7, pp. 2029–2039, Jul. 2012.
[59] Y. Zhao, J. Wu, and S. Lu, "Throughput maximization in cognitive radio based wireless mesh networks," in *Proc. Mil. Commun. Conf. (MILCOM)*, Nov. 2011, pp. 260–265.
[60] L. Venturino, N. Prasad, and X. Wang, "Coordinated scheduling and power allocation in downlink multicell OFDMA networks," *IEEE Trans. Veh. Technol.*, vol. 58, no. 6, pp. 2835–2848, Jun. 2009.
[61] G. Li, H. Chen, and J. Cai, "Joint user association and power allocation for hybrid half-duplex/full-duplex relaying in cellular networks," *IEEE Syst. J.*, vol. 13, no. 2, pp. 1145–1156, Jun. 2019.
[62] T. V. Chien, E. Lagunas, T. H. Ta, S. Chatzinotas, and B. Ottersten, "User scheduling and power allocation for precoded multi-beam high throughput satellite systems with individual quality of service constraints," 2021, *arXiv:2110.02525*.
[63] R. A. Horn and C. R. Johnson, *Matrix Analysis*. Cambridge, U.K.: Cambridge Univ. Press, 1985.
[64] S. Boyd and L. Vandenberghe, *Convex Optimization*. Cambridge, U.K.: Cambridge Univ. Press, 2004.
[65] M. Rahman and H. Yanikomeroglu, "Enhancing cell-edge performance: A downlink dynamic interference avoidance scheme with inter-cell coordination," *IEEE Trans. Wireless Commun.*, vol. 9, no. 4, pp. 1414–1425, Apr. 2010.